← 이제 방법론의 적용에 들어감 (12장)

2차 13장 Earthquake Analysis of Linear Systems

- Response History Analysis (RHA)
- Response Spectrum Analysis (RSA)

RHA ← modal analysis (2차 12장에서 일반적과 이번 취급) "specialization"

① Eq. of motion

$$m\ddot{u} + c\dot{u} + ku = p_{eff}(t)$$

$$p_{eff}(t) = -m\iota\ddot{u}_g(t)$$

ι = influence vector, 통상 {1} for usual bldg structures

② Modal expansion of displacements and forces

$$u(t) = \sum \phi_n q_n(t)$$

$$s = m\iota = \sum s_n = \sum \Gamma_n m \phi_n$$

「유효지진하중의 공간적 분포 (unit ground accel.)」

where $\Gamma_n = \dfrac{L_n}{M_n}$

Γ_n $\quad L_n = \phi_n^T m \iota$, $M_n = \phi_n^T m \phi_n$

$$s_n = \left(\frac{L_n}{M_n}\right) m\phi_n = \frac{\phi_n^T [m\iota m]\phi_n}{\phi_n^T m \phi_n}$$

「ϕ_n의 normalization 방법과 무관하게 unique한 값이 얻어짐을 주목」

③ Modal equations

$$\ddot{q}_n + 2\xi_n\omega_n\dot{q}_n + \omega_n^2 q_n = -\Gamma_n \ddot{u}_g(t)$$

$$\ddot{D}_n + 2\xi_n\omega_n\dot{D}_n + \omega_n^2 D_n = -\ddot{u}_g(t)$$

$$q_n(t) = \Gamma_n D_n(t)$$;

④ Modal responses

$$\underline{u}_n(t) = \underline{\phi}_n \cdot q_n(t) = \underline{\phi}_n \cdot \Gamma_n \cdot D_n(t)$$

Equivalent static forces due to the n^{th} mode,

$$\underline{f}_n(t) = \underline{k}\,\underline{u}_n(t) = \underline{k}\,\underline{\phi}_n \Gamma_n D_n(t)$$

$$= \Gamma_n (\omega_n^2 \underline{m}\,\underline{\phi}_n) D_n(t)$$

$$= \Gamma_n \underline{m}\,\underline{\phi}_n (\omega_n^2 D_n(t)) = \underline{s}_n \times A_n(t)$$

($\underline{s}_n$: $A_n(t)$)

↳ see Fig. 13.1.1 (P. 512)

$$r_n(t) = r_n^{st} \times A_n(t)$$

↳ $\underline{s}_n$을 가하여 얻어진 정적인 응답

⑤ Total response

$$\underline{u}(t) = \sum \underline{u}_n(t) = \sum \Gamma_n \underline{\phi}_n D_n(t)$$

$$r(t) = \sum r_n(t) = \sum r_n^{st} \cdot A_n(t)$$

↳ (N개의 강성행렬 ← $\underline{s}_n$ $(n=1, 2, \cdots, N)$
plus
N개의 SDF의 동적해석)

P. 512 (Fig. 13.1.1 참조).

(가장 중요 (기본))

☆ 「Specialization of modal analysis for multistory buildings with symm. plan」 ← 13.2장

↓ Fig. 13.2-1 (p. 518)

No torsion → 예시 없이 바로 특화시 봄 (easy to follow)

Eq. of motion

$$\underline{m}\,\ddot{\underline{u}} + \underline{c}\,\dot{\underline{u}} + \underline{k}\,\underline{u} = -\underline{m}\{1\}\ddot{u}_g \quad , \text{or} \ldots \ \underline{\iota} = \{1\}$$

Modal expansion of $\underline{P}_{eff}(t)$

$$\underline{s} = \underline{m}\{1\} = \sum \underline{s}_n = \sum \Gamma_n \underline{m}\,\underline{\phi}_n$$

$$\Gamma_n = \frac{L_n^h}{M_n} = \frac{\underline{\phi}_n^T \underline{m}\{1\}}{\underline{\phi}_n^T \underline{m}\,\underline{\phi}_n} = \frac{\sum_{j=1}^{N} m_j \phi_{jn}}{\sum_{j=1}^{N} m_j \phi_{jn}^2}$$

$$\underline{s}_n = \Gamma_n \underline{m}\,\underline{\phi}_n \quad \text{or} \quad s_{jn} = \Gamma_n m_j \phi_{jn}$$

Modal responses

$$u_{jn}(t) = \Gamma_n \phi_{jn} D_n(t)$$

주목할 점! 층간변위 결정은 Eigen vecter

(Inter) story Drift → $\Delta_{jn}(t) = u_{jn} - u_{(j-1)n} = \Gamma_n(\phi_{jn} - \phi_{j-1,n}) D_n(t)$

Equivalent static forces → $\underline{f}_n(t) = \underline{s}_n \times A_n(t)$ or $f_{jn}(t) = s_{jn} \cdot A_n(t)$

Any response → $r_n(t) = r_n^{st} \times A_n(t)$

↳ due to $\underline{s}_n$

"Six response quantities" from the nth "modal static" response

↳ Table 13.2-1 참조, p.510 ; Fig. 13.2-2, p.511

★ Close follow-up 요!

✓ ① ith story shear V_{in}^{st}

② ith story overturning moment M_{in}^{st}

✓ ③ base shear V_{bn}^{st}

✓ ④ base overturning moment M_{bn}^{st}

✓ ⑤ floor displ. u_{jn}^{st}

✓ ⑥ story drift Δ_{jn}^{st}

See Fig. 13.2.2 (p.511)

Note: ③ $V_{bn}^{st} = \sum_{j=1}^{N} s_{jn} = \underset{1\times N}{\underline{s}_n^T} \underset{N\times 1}{\{1\}}$

$\{1\} = \sum_j x_j \underline{\phi}_j \rightarrow \underline{\phi}_n^T \underline{m}\{1\} = \underline{\phi}_n^T \underline{m}\left(\sum_j x_j \underline{\phi}_j\right)$

$= \sum_{n=1}^{N} \frac{L_n^h}{M_n} \cdot \underline{\phi}_n$

$L_n^h = x_n \cdot M_n$ or $x_n = \Gamma_n = \frac{L_n^h}{M_n}$

(modal expansion of $\{1\}$)

$\underline{L}_n$

• $\underline{s}_n^T = (\Gamma_n \underline{m} \underline{\phi}_n)^T = \Gamma_n \underline{\phi}_n^T \underline{m}$ a.k.

$\therefore V_{bn}^{st} = \underbrace{\Gamma_n \underline{\phi}_n^T \underline{m}}_{\underline{s}_n^T} \left(\sum_{r=1}^{N} \frac{L_r^h}{M_r} \underline{\phi}_r\right) \{1\}$

$= \Gamma_n \cdot \frac{L_n^h}{M_n} \cdot M_n = \Gamma_n \cdot L_n^h \equiv M_n^*$

(Note: unit acceleration 일 때만 성립한다)

n차 모드의 유효질량 (다음 쪽 참조)

$\underline{h} = \sum_m x_m \underline{\phi}_m$

$\underline{\phi}_r^T \underline{m} \underline{h} = \underline{\phi}_r^T \underline{m} \sum x_m \underline{\phi}_m$

$= M_r \cdot x_m$

$\therefore x_m = \frac{\underline{\phi}_r^T \underline{m} \underline{h}}{M_r} \leftarrow L_r$

← story height vector

④ $M_{bn}^{st} = \underline{s}_n^T \cdot \underline{h}$

$= (\Gamma_n \underline{\phi}_n^T \underline{m}) \cdot \left(\sum_{r=1}^{N} \frac{L_r^\theta}{M_r} \underline{\phi}_r\right)$ ← $L_r^\theta = \underline{\phi}_r^T \underline{m} \underline{h}$

$= \Gamma_n \times \frac{L_n^\theta}{M_n} \times M_n$

$\therefore M_{bn}^{st} = \Gamma_n \times L_n^\theta = \underbrace{(\Gamma_n L_n^h)}_{M_n^*} \left(\frac{L_n^\theta}{L_n^h}\right) \equiv M_n^* \times h_n^*$

n차 모드의 질량 (다음 쪽 참조) ← 유효높이

Total response

$$r(t) = \sum_{n=1}^{N} r_n(t) = \sum_{n=1}^{N} r_n^{st} \times A_n(t)$$

"Effective modal mass and modal height" ; M_n^*, h_n^*

↑ p. 523, Fig. 13.2.3 참조

$$V_{bn} = V_{bn}^{st} \times A_n(t)$$

$$= (\Gamma_n \cdot L_n^h) \times A_n(t) = M_n^* \cdot A_n(t)$$

- Γ_n: n차 모드의 탄성변형에 의한 상량
- L_n^h: 가속도 응답
- M_n^*: 유효질량

Note: $\sum_{n=1}^{N} M_n^* = \sum_{j=1}^{N} m_j$ 관계가 성립.

증명:

$$\underline{M}\{1\} = \sum_{n=1}^{N} \Gamma_n \underline{M} \underline{\phi}_n \leftarrow \{1\} = \sum \Gamma_n \times \underline{\phi}_n \text{ 이므로}$$

$$\{1\}^T \underline{M} \{1\} = \sum_{n=1}^{N} \Gamma_n \{1\}^T \underline{M} \underline{\phi}_n$$

- $\{1\}^T \underline{M} \{1\}$: total mass의 상량 ($\underline{M}$ = 대각성분 행렬)
- $\{1\}^T \underline{M} \underline{\phi}_n$: $(L_n^h)^T$의 상량

$$\sum_{j=1}^{N} m_j = \sum_{n=1}^{N} \Gamma_n \cdot L_n^h$$

M_n^*

$(L_n^h)^T = L_n^h$ (scalar 양이므로)

$\therefore \sum_{n=1}^{N} M_n^*$ (대각) $= \sum_{j=1}^{N} m_j$ (전체)

($n=1$: 모드방향, j: 질량방향)

Note!: 모드방향 질량방향

$$M_{bn} = M_{bn}^{st} A_n(t)$$

$$= (\Gamma_n \cdot L_n^{\theta}) A_n(t)$$

$$= (\underbrace{\Gamma_n \cdot L_n^h}_{M_n^*} \times \frac{L_n^{\theta}}{L_n^h}) \times A_n(t)$$

$$h_n^* = \frac{\phi_n^T m\, h}{\phi_n^T m \{1\}} \qquad \phi_n^T m\, h = L_n^{\theta} \leftarrow \text{base moment}, \qquad \phi_n^T m \{1\} = L_n^h$$

↑ 총 횡력의 크기

"바리뇽의 정리를 생각해 볼 것"

$$\underbrace{M_{bn}}_{\text{base overturning moment}} = \underbrace{(\underbrace{\Gamma_n \cdot L_n^h}_{M_n^*} \times A_n(t))}_{\text{base shear}} \times \underbrace{\frac{L_n^{\theta}}{L_n^h}}_{= h_n^*}$$

base overturning moment

base shear (= 횡력의 合)

n차 모드 질량의 유효높이에 상당

Note: $\sum_{j=1}^{N} h_j m_j = \sum_{n=1}^{N} h_n^* M_n^*$ ← 증명가능 pp. 524~525

("13.2.6 절 예제 follow-up 요" 참고)

~~RSA ← pp. 555~574~~ 520

~~(기타 공부할 것)~~

과제 13.1 and 13.2
↓
임의의 상용프로그램 사용할 것 (가령 NONSPEC, SAP 2000, … any)

Response Spectrum Analysis

↓

Noting that $\mathbf{m}$ is a diagonal matrix with $m_{jj} = m_j$, this can be rewritten as

$$\sum_{j=1}^{N} m_j h_j = \sum_{n=1}^{N} \frac{L_n^\theta}{M_n} L_n^h = \sum_{n=1}^{N} h_n^* M_n^*$$

wherein Eq. (13.2.9) has been used. This provides a proof for Eq. (13.2.17).

Example 13.5

Determine the effective modal masses and effective modal heights for the two-story shear frame of Example 13.2. The height of each story is h.

Solution In Example 13.2 the $\mathbf{m}$, $\mathbf{k}$, ω_n, and ϕ_n for this system were presented, and L_n^h and M_n for each of the two modes computed. These are listed next, together with the new computations for M_n^* and h_n^*. For the first mode: $L_1^h = 2m$, $M_1 = 3m/2$, $M_1^* = (L_1^h)^2/M_1 = \frac{8}{3}m$, $L_1^\theta = h(2m)\frac{1}{2} + 2h(m)1 = 3hm$, and $h_1^* = L_1^\theta/L_1^h = 3hm/2m = 1.5h$. Similarly, for the second mode: $L_2^h = -m$, $M_2 = 3m$, $M_2^* = (L_2^h)^2/M_2 = \frac{1}{3}m$, $L_2^\theta = h(2m)(-1) + 2h(m)1 = 0$, and $h_2^* = L_2^\theta/L_2^h = 0$.

Observe that $M_1^* + M_2^* = 3m$, the total mass of the frame, confirming that Eq. (13.2.14) is satisfied; also note that the effective height for the second mode is zero, implying that the base overturning moment $M_{b2}(t)$ due to that mode will be zero at all t. This is an illustration of a more general result developed in Example 13.6.

Example 13.6

Show that the base overturning moment in a multistory building due to the second and higher modes is zero if the first mode shape is linear (i.e., the floor displacements are proportional to floor heights above the base).

Solution Equation (13.2.15) gives the nth-mode contribution to the base overturning moment. A linear first mode implies that $\phi_{j1} = h_j/h_N$, where h_j is the height of the jth floor above the base and h_N is the total height of the building. Substituting $h_j = h_N \phi_{j1}$ in (13.2.9b) gives

$$L_n^\theta = \sum_{j=1}^{N} h_j m_j \phi_{jn} = h_N \phi_1^T \mathbf{m} \phi_n$$

and this is zero for all $n \neq 1$ because of the orthogonality property of modes. Therefore, for all $n \neq 1$, $h_n^* = 0$ from Eq. (13.2.9a) and $M_{bn}(t) = 0$ from Eq. (13.2.15).

13.2.6 Example: Five-Story Shear Frame

In this section the earthquake analysis procedure summarized in Section 13.2.4 is implemented for the five-story shear frame of Fig. 12.8.1, subjected to the El Centro ground motion shown in Fig. 6.1.4. The results presented are accompanied by interpretive comments that should assist us in developing an understanding of the response behavior of multistory buildings.

System properties. The lumped mass $m_j = m = 100$ kips/g at each floor, the lateral stiffness of each story is $k_j = k = 31.54$ kips/in., and the height of each

story is 12 ft. The damping ratio for all natural modes is $\zeta_n = 5\%$. The mass matrix $\mathbf{m}$, stiffness matrix $\mathbf{k}$, natural frequencies, and natural modes of this system were presented in Section 12.8. For the given k and m, the natural periods are $T_n = 2.0, 0.6852, 0.4346, 0.3383$, and 0.2966 sec. (These natural periods, which are much longer than for typical five-story buildings, were chosen to accentuate the contributions of the second through fifth modes to the structural response.) Thus steps 1, 2, and 3 of the analysis procedure (Section 13.2.4) have already been completed.

Modal expansion of m1. To implement step 4 of the analysis procedure (Section 13.2.4), the modal properties M_n, L_n^h, and L_n^θ are computed from Eqs. (13.2.3) and (13.2.9b) using the known modes ϕ_n (Table 13.2.2). The Γ_n are computed from Eq. (13.2.3)

TABLE 13.2.2 MODAL PROPERTIES

Mode	M_n	L_n^h	L_n^θ/h
1	1.000	1.067	3.750
2	1.000	−0.336	0.404
3	1.000	0.177	0.135
4	1.000	−0.099	0.059
5	1.000	0.045	0.023

and substituted in Eq. (13.2.4), together with values for m_j and ϕ_{jn}, to obtain the $\mathbf{s}_n$ vectors shown in Fig. 13.2.4. Observe that the direction of forces $\mathbf{s}_n$ is controlled by the algebraic sign of ϕ_{jn} (Fig. 12.8.2). Hence, these forces for the fundamental mode act in the same direction, but for the second and higher modes they change direction as one moves up the structure. The contribution of the fundamental mode to the force distribution $\mathbf{s} = \mathbf{m1}$ of the effective earthquake forces is the largest, and the modal contributions to these forces decrease progressively for higher modes.

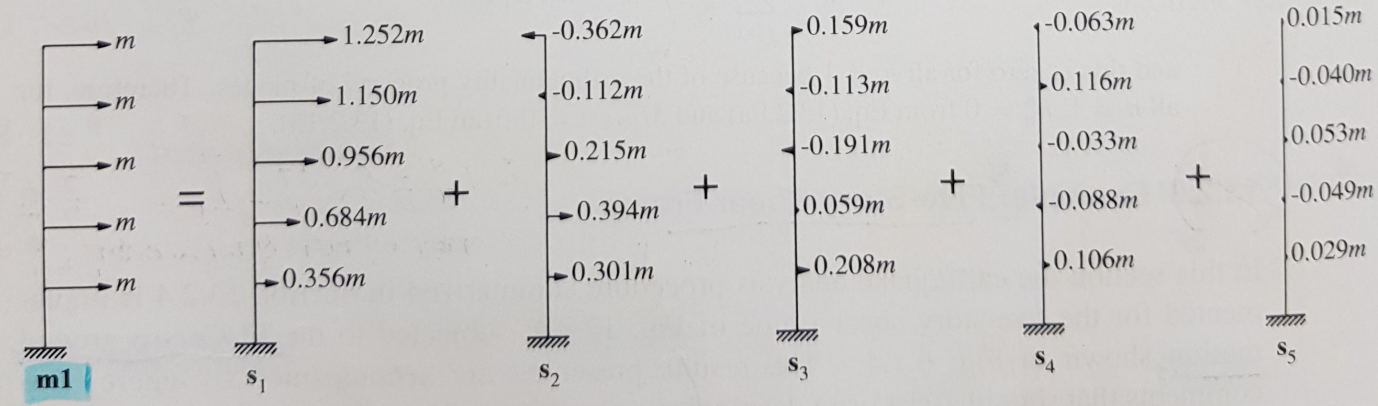

Figure 13.2.4 Modal expansion of **m1**.

Modal static responses. Table 13.2.3 gives the results for four response quantities—base shear V_b, fifth-story shear V_5, base overturning moment M_{bn}, and roof

TABLE 13.2.3 MODAL STATIC RESPONSES

Mode	V_{bn}^{st}/m	V_{5n}^{st}/m	M_{bn}^{st}/mh	u_{5n}^{st}
1	4.398	1.252	15.45	0.127
2	0.436	−0.362	−0.525	−0.004
3	0.121	0.159	0.092	0.0008
4	0.037	−0.063	−0.022	−0.0002
5	0.008	0.015	0.004	0.00003

displacement u_5—obtained using the equations in Table 13.2.1 and the known s_{jn}, ϕ_{5n}, and ω_n^2 (step 5a of Section 13.2.4). Observe that the modal static responses are largest for the first mode and decrease progressively for higher modes. The effective modal masses $M_n^* = V_{bn}^{st}$ and effective modal heights $h_n^* = M_{bn}^{st}/V_{bn}^{st}$ are shown schematically in Fig. 13.2.5; note that h_n^* are plotted without their algebraic signs. Observe that $\sum M_n^* = 5m$, confirming that Eq. (13.2.14) is satisfied. Also note that $\sum h_n^* M_n^* = 15mh$; this is the same as $\sum h_j m_j = 15mh$, confirming that Eq. (13.2.17) is satisfied.

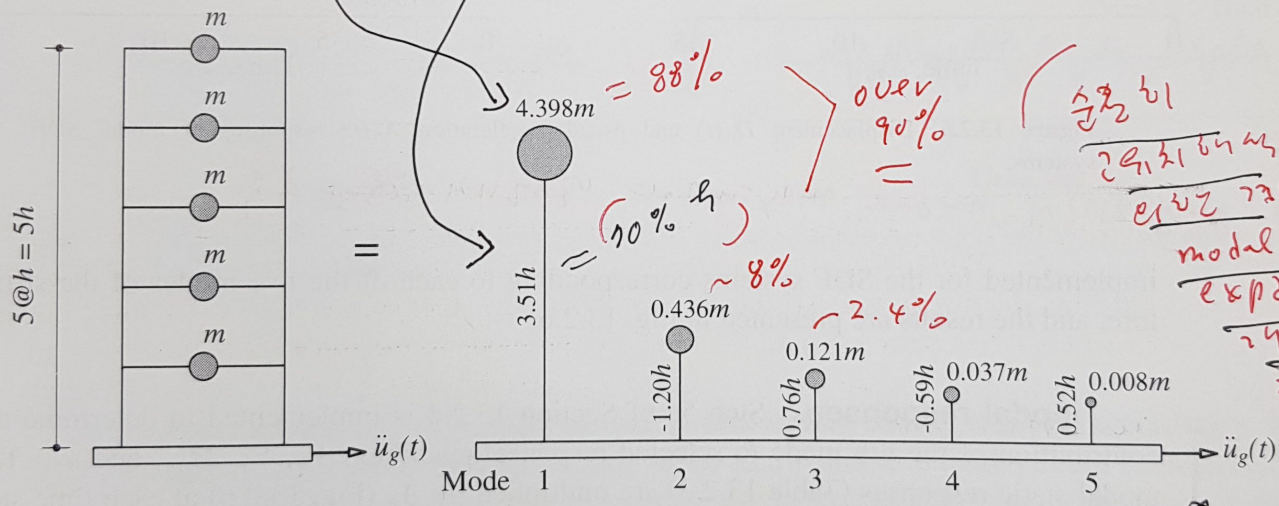

Figure 13.2.5 Effective modal masses and effective modal heights.

Earthquake excitation. The ground acceleration $\ddot{u}_g(t)$ is defined by its numerical values at time instants equally spaced at every Δt. This time step $\Delta t = 0.01$ sec is chosen to be small enough to define $\ddot{u}_g(t)$ accurately and to determine accurately the response of SDF systems with natural periods T_n, the shortest of which is 0.2966 sec.

Response of SDF systems. The deformation response $D_n(t)$ of the nth-mode SDF system with natural period T_n and damping ratio ζ_n to the ground motion is determined (step 5b of Section 13.2.4). The time-stepping linear acceleration method (Chapter 5) was implemented to obtain discrete values of D_n at every Δt. For convenience, however, we continue to denote these discrete values as $D_n(t)$. At each time instant the pseudo-acceleration is calculated from $A_n(t) = \omega_n^2 D_n(t)$. These computations are

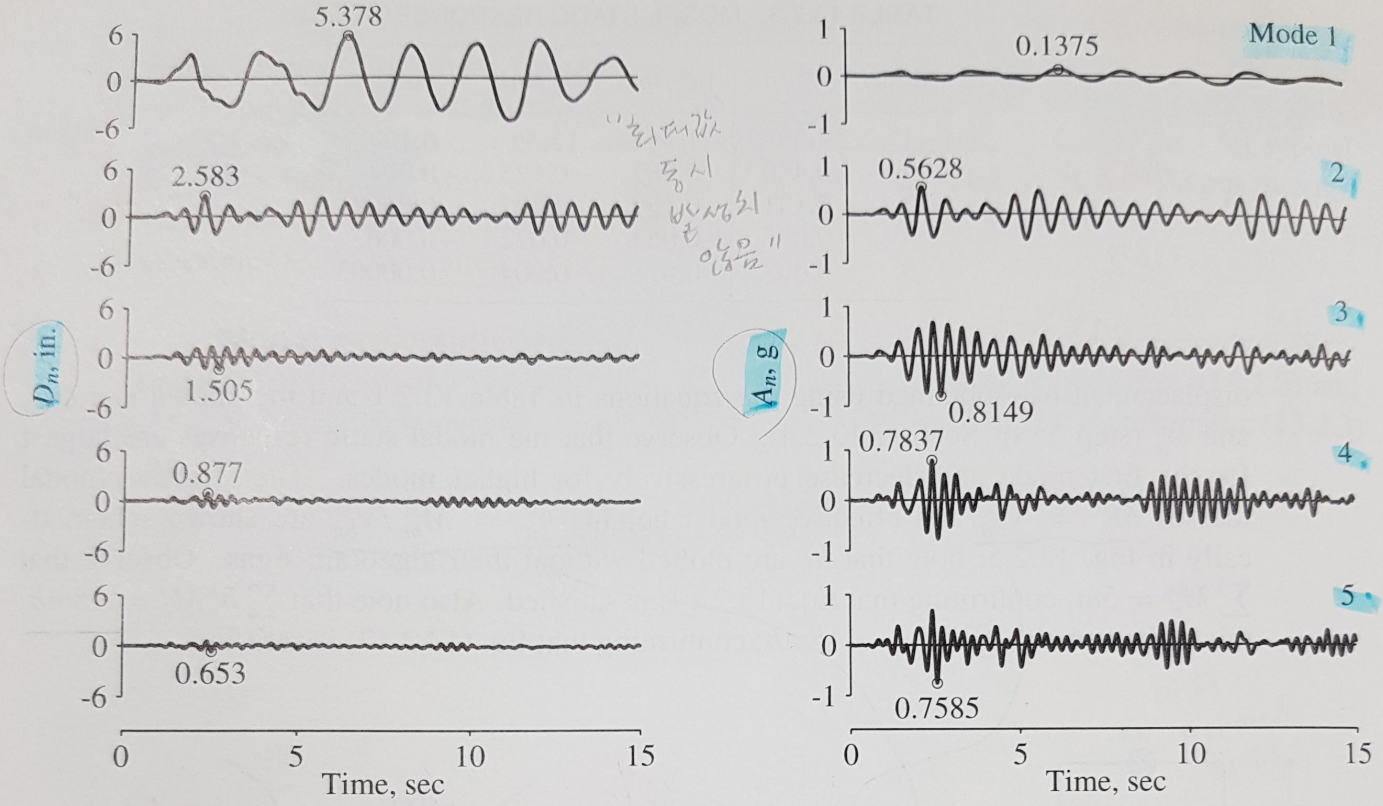

Figure 13.2.6 Displacement $D_n(t)$ and pseudo-acceleration $A_n(t)$ responses of modal SDF systems.

implemented for the SDF systems corresponding to each of the five modes of the structure, and the results are presented in Fig. 13.2.6.

Modal responses. Step 5c of Section 13.2.4 is implemented to determine the contribution of the nth mode to selected response quantities: V_b, V_5, M_{bn}, and u_5. The modal static responses (Table 13.2.3) are multiplied by A_n (Fig. 13.2.6) at each time step to obtain the results presented in Figs. 13.2.7 and 13.2.8.

These results give us a first impression of the relative values of the response contributions of the various modes. The modal static responses (Table 13.2.3) had suggested that the response will be largest in the fundamental mode and will tend to decrease in the higher modes. Such is the case in this example for roof displacement, base shear, and base overturning moment but not for the fifth-story shear. How the relative modal responses depend on the response quantity and on the building properties is discussed in Chapter 18.

Total responses. The total responses, determined by combining the modal contributions $r_n(t)$ (step 6 of Section 13.2.4) according to Eq. (13.2.10), are shown in Figs. 13.2.7 and 13.2.8. The results presented indicate that it is not necessary to include the contributions of all the modes in computing the response of a multistory building; the

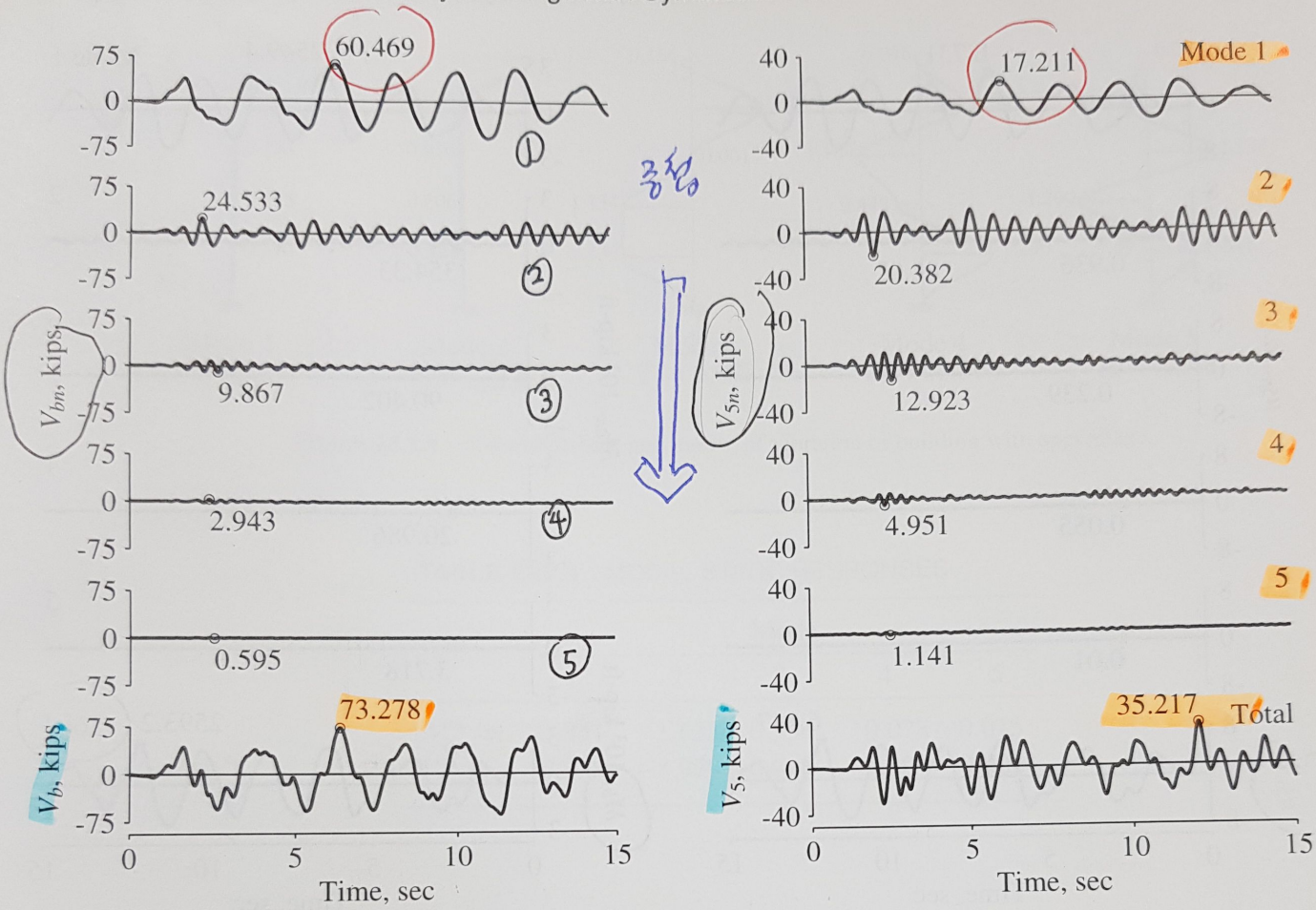

Figure 13.2.7 Base shear and fifth-story shear: modal contributions, $V_{bn}(t)$ and $V_{5n}(t)$, and total responses, $V_b(t)$ and $V_5(t)$.

lower few modes may suffice and the modal summations can be truncated accordingly. In this particular example, the contribution of the fourth and fifth modes could be neglected; the results would still be accurate enough for use in structural design. How many modes should be included depends on the earthquake ground motion and building properties. This issue is addressed in Chapter 18.

Before leaving this example, we make three additional observations that will be especially useful in Part B of this chapter. First, as seen in Chapter 6, the peak values of $D_n(t)$ and $A_n(t)$, noted in Fig. 13.2.6, can be determined directly from the response spectrum for the ground motion. This fact will enable us to determine the peak value of the nth-mode contribution to any response quantity directly from the response spectrum. Second, the contribution of the nth mode to every response quantity attains its peak value at the same time as $A_n(t)$ does. Third, the peak value of the total response occurs at a time instant different from when the individual modal peaks are attained. Furthermore, the peak values of the total responses for the four response quantities occur at different time instants because the relative values of the modal contributions vary with the response quantity.

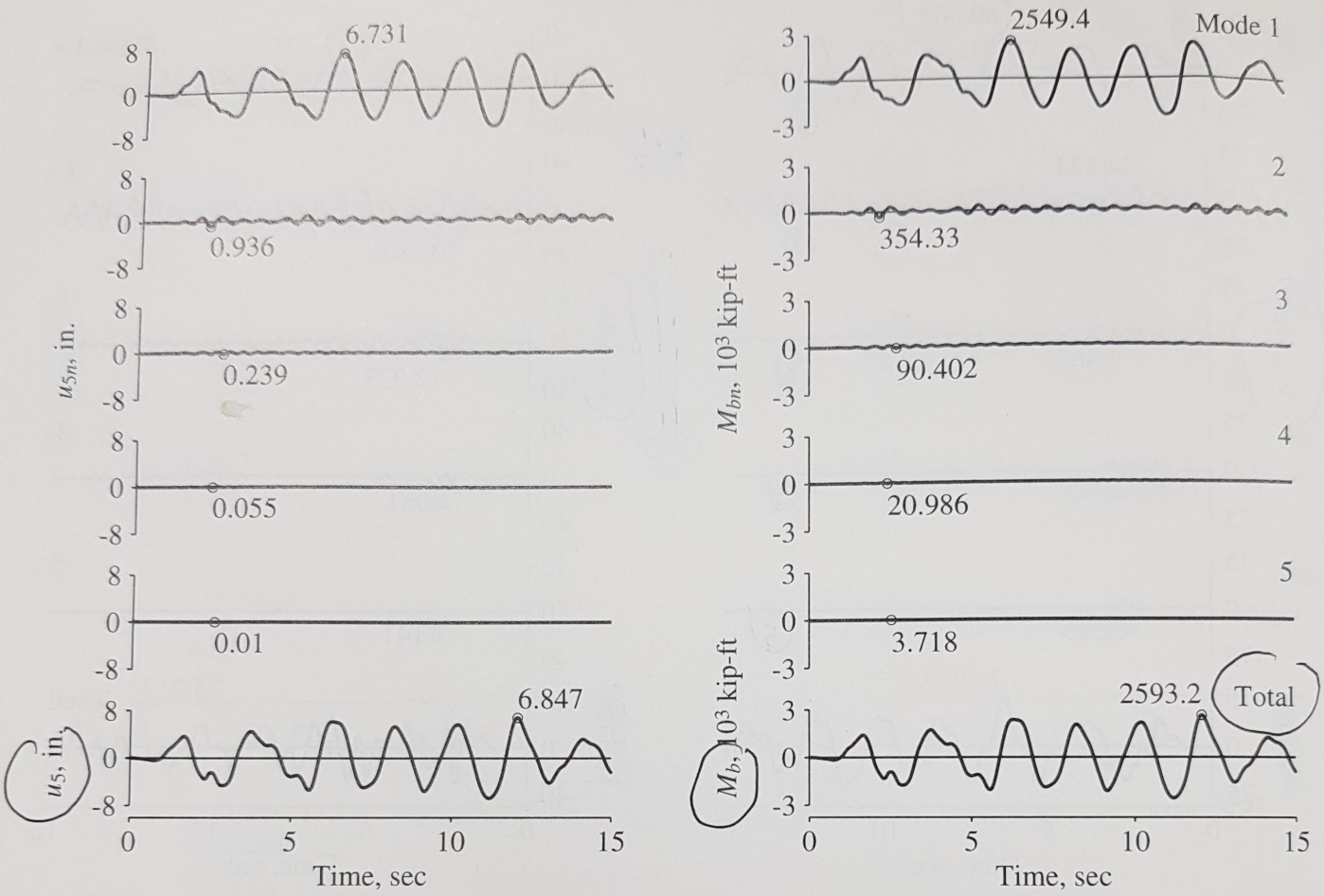

Figure 13.2.8 Roof displacement and base overturning moment: modal contributions, $u_{5n}(t)$ and $M_{bn}(t)$, and total responses, $u_5(t)$ and $M_b(t)$.

13.2.7 Example: Four-Story Frame with an Appendage

This section is concerned with the earthquake analysis and response of a four-story building with a light appendage—a penthouse, a small housing for mechanical equipment, an advertising billboard, or the like. This example is presented because it brings out certain special response features representative of a system with two natural frequencies that are close.

System properties. The lumped masses at the first four floors are $m_j = m$, the appendage mass $m_5 = 0.01m$, and $m = 100$ kips/g. The lateral stiffness of each of the first four stories is $k_j = k$, the appendage stiffness $k_5 = 0.0012k$, and $k = 22.599$ kips/in. The height of each story and the appendage is 12 ft. The damping ratio for all natural modes is $\zeta_n = 5\%$. The response of this system to the El Centro ground motion is determined. The analysis procedure and its implementation are identical to Section 13.2.6; therefore, only a summary of the results is presented.

where $D(t, \omega_y, \zeta)$ and $A(t, \omega_y, \zeta)$ denote the deformation and pseudo-acceleration responses, respectively, of an SDF system with natural frequency ω_y and damping ratio ζ to ground acceleration $\ddot{u}_{gy}(t)$. Frames B and C would experience no forces.

For the symmetric-plan system associated with Example 13.8, $\omega_y = 6.344$ (see Example 10.7) and the damping ratio is the same, $\zeta = 5\%$. The response of this SDF system is computed from Eqs. (a) to (c) and shown in Fig. E13.9, where it is also compared with the response of the unsymmetric-plan system (Example 13.8). It is clear that plan asymmetry has the effect of (1) modifying the lateral displacement and base shear in frame A, and (2) causing torsion in the system and forces in frames B and C that do not exist if the building plan is symmetric. In this particular case, the base shear in frame A is reduced because of plan asymmetry, but such is not always the case, depending on the natural period of the structure, ground motion characteristics, and the location of the frame in the building plan.

13.4 TORSIONAL RESPONSE OF SYMMETRIC-PLAN BUILDINGS

In this section the torsional response of multistory buildings with their plans nominally symmetric about two orthogonal axis is discussed briefly. Such structures may undergo "accidental" torsional motions for mainly two reasons: the building is usually not *perfectly* symmetric, and the spatial variations in ground motion may cause rotation (about the vertical axis) of the building's base, which will induce torsional motion of the building even if its plan is perfectly symmetric.

Consider first the analysis of torsional response of a building with a perfectly symmetric plan due to rotation of its base. For a given rotational excitation $\ddot{u}_{g\theta}(t)$, the governing equations (9.6.1) can be solved by the modal analysis procedure, considering only the purely torsional vibration modes of the building. This procedure could be developed along the lines of Section 13.3. It is not presented, however, for two reasons: (1) it is straightforward; and (2) in structural engineering practice, buildings are not analyzed for rotational excitation. Therefore, in this brief section we present the results of such analysis and compare them with building torsion recorded during an earthquake.

Consider the building shown in Fig. 13.4.1, located in Pomona, California. This reinforced-concrete frame building has two stories, a partial basement and a light penthouse structure. For all practical and code design purposes, the building has a nominally symmetric floor plan, as indicated by its framing plan in Fig. 13.4.2. The lateral force-resisting system in the building consists of peripheral columns interconnected by longitudinal and transverse beams, but the L-shaped exterior corner columns as well as the interior columns in the building are not designed especially for earthquake resistance. The floor decking system is formed by a 6-in.-thick concrete slab. The building also includes walls in the stairwell system—concrete walls in the basement and masonry walls in upper stories. Foundations of columns and interior walls are supported on piles.

The accelerograph channels located as shown in Fig. 13.4.3 recorded the motion of the building during the Upland (February 28, 1990) earthquake, including three channels of horizontal motion at each of three levels: roof, second floor, and basement. The peak accelerations of the basement were 0.12g and 0.13g in the x and y directions, respectively.

Figure 13.4.1 First Federal Savings building, a two-story reinforced-concrete building (with a partial basement) in Pomona, California. (Courtesy of California Strong Motion Instrumentation Program.)

These motions were amplified to 0.24g in the x-direction and 0.39g in the y-direction at the roof. The building experienced no structural damage during this earthquake.

Some of the recorded motions are shown in Fig. 13.4.4. These include the x-translational accelerations at two locations at the basement of the building and at two locations at the roof level. By superimposing the motions at two locations on the roof in Fig. 13.4.5 it is clear that this building experienced some torsion; otherwise, these two motions would have been identical. Assuming rigid base, its rotational acceleration is computed as the difference between the two x-translational records at the basement of the building divided by the distance between the two locations. This rotational base acceleration is multiplied by $b/2$, where the building-plan dimension $b = 109.75$ ft, and plotted in Fig. 13.4.6. The peak value of $(b/2)\ddot{u}_{g\theta}(t)$ is 0.029g compared with the peak acceleration of 0.12g in the x-direction.

The torsional response of the building to the rotational motion of the basement, Fig. 13.4.6, is determined by modal solution of Eq. (9.6.1) with modal damping ratios of 5%. These damping ratios were estimated from the recorded motions at the roof and basement using some of the procedures mentioned in Chapter 11, Part A. The response history of the shear force in a selected column of the building is presented in Fig. 13.4.7. This is only a part of the element force due to the actual torsional motion of the building during the earthquake, as will be demonstrated next.

Approximate values of the element forces due to recorded torsion can be determined at each instant of time by static analysis of the building subjected to floor inertia torques $I_{Oj}\ddot{u}^t_{j\theta}(t)$ at all floors ($j = 1, 2, \ldots, N$), where I_{Oj} is the moment of inertia of the jth floor mass about the vertical axis through O, the center of mass (CM) of the floor, and

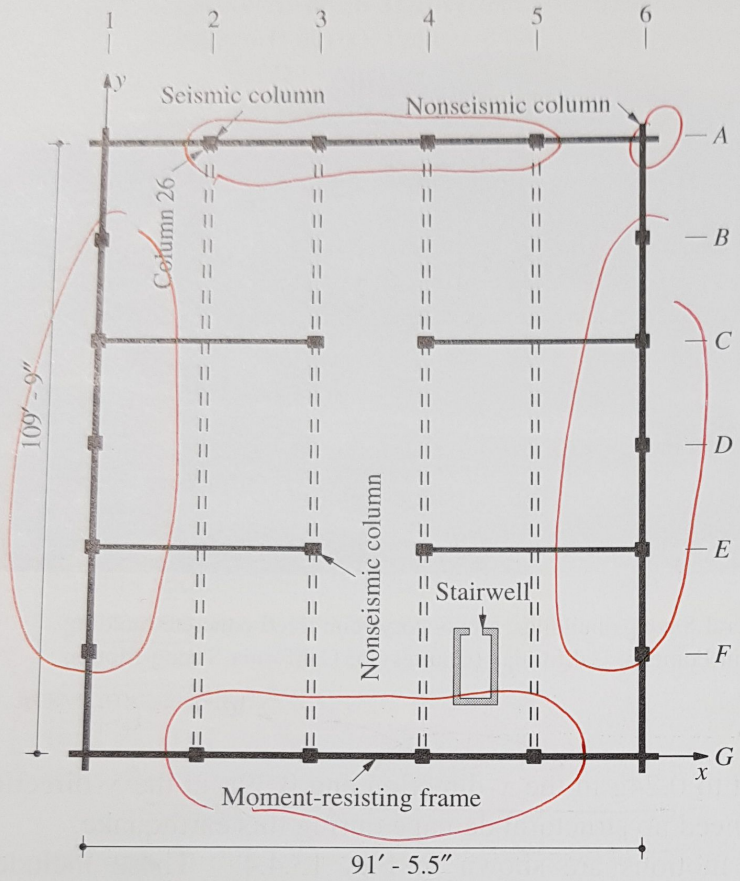

Figure 13.4.2 Framing plan of First Federal Savings building.

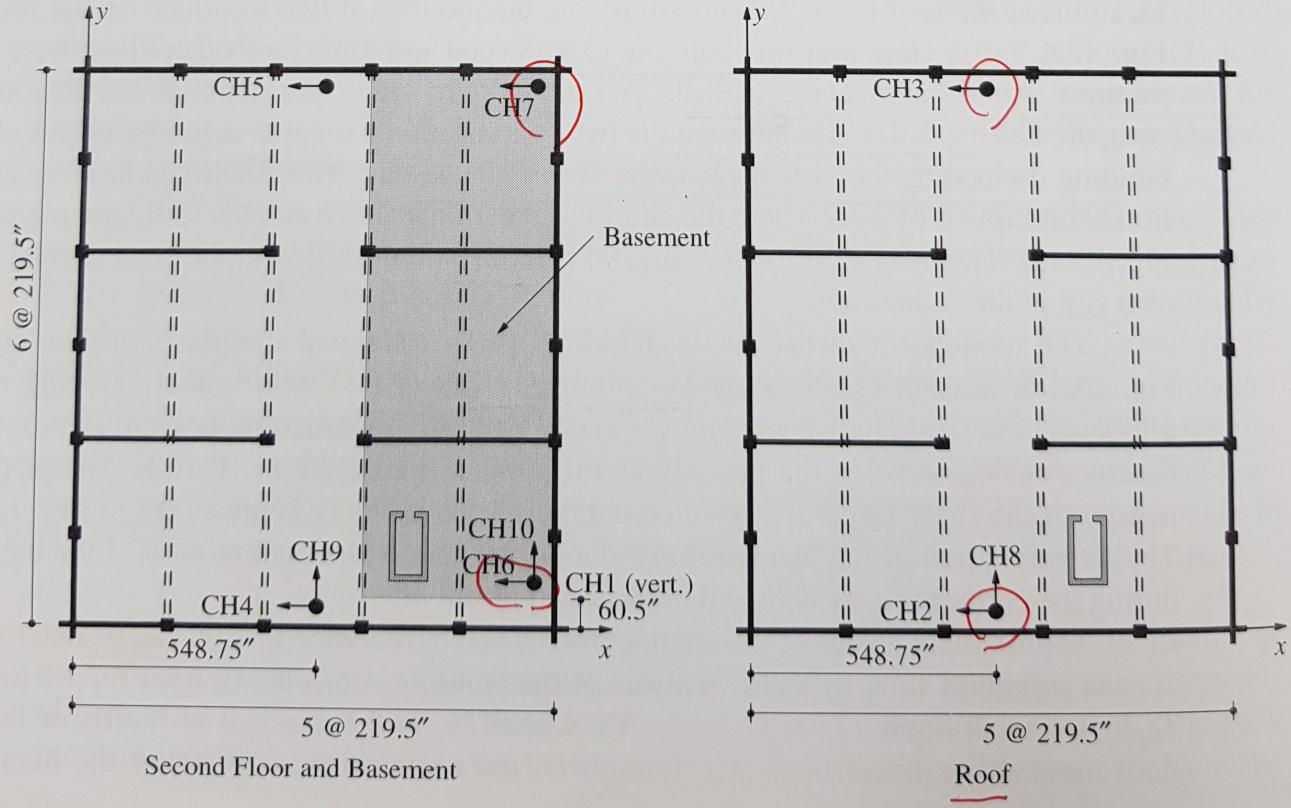

Figure 13.4.3 Accelerograph channels in First Federal Savings building.

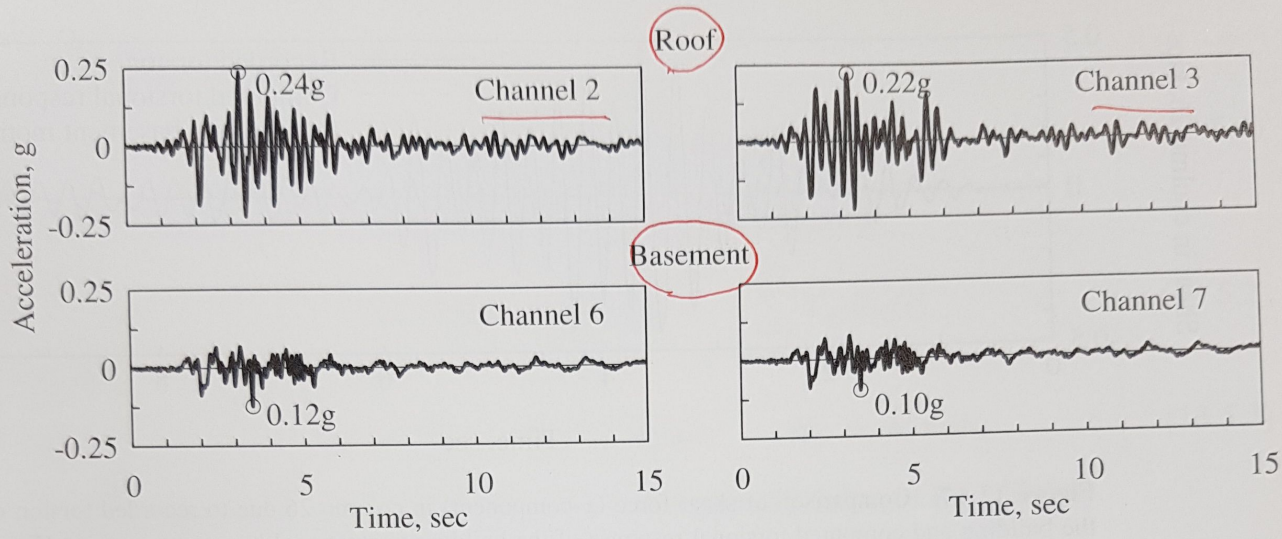

Figure 13.4.4 Motions recorded at First Federal Savings building during the Upland earthquake of February 28, 1990.

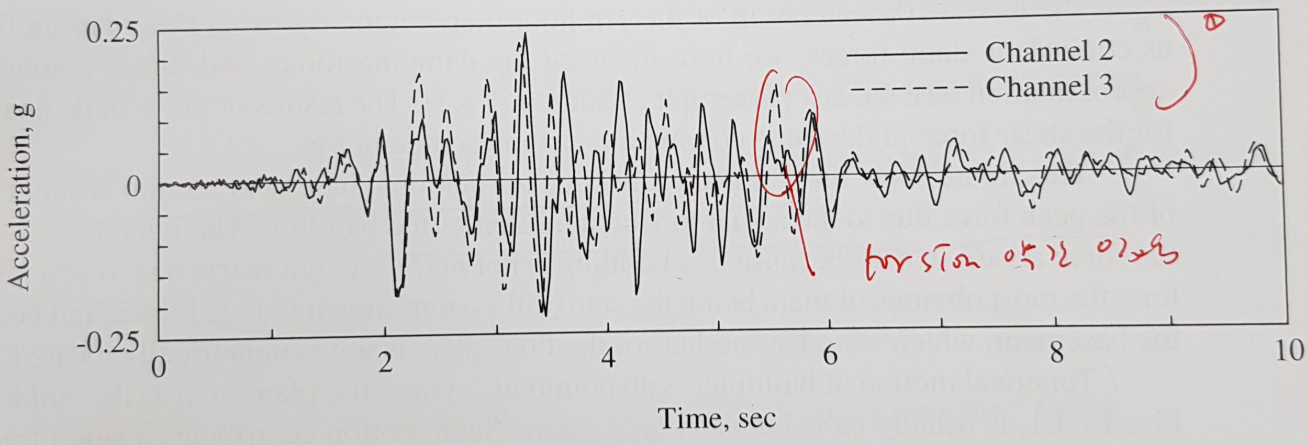

Figure 13.4.5 Motions recorded at two locations on the roof of First Federal Savings building during the Upland earthquake of February 28, 1990.

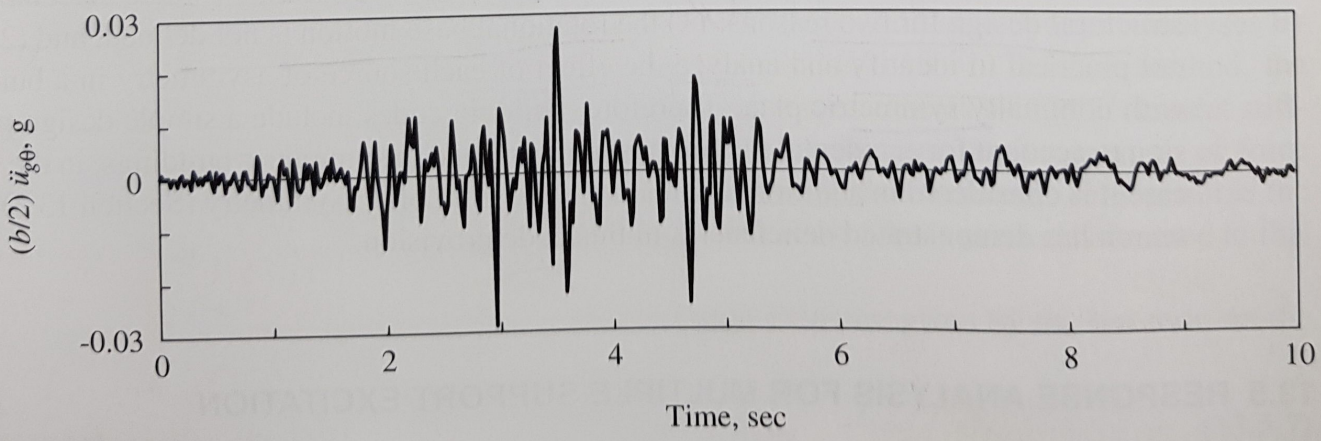

Figure 13.4.6 Rotational acceleration of basement multiplied by $b/2$. [From De la Llera and Chopra (1994).]

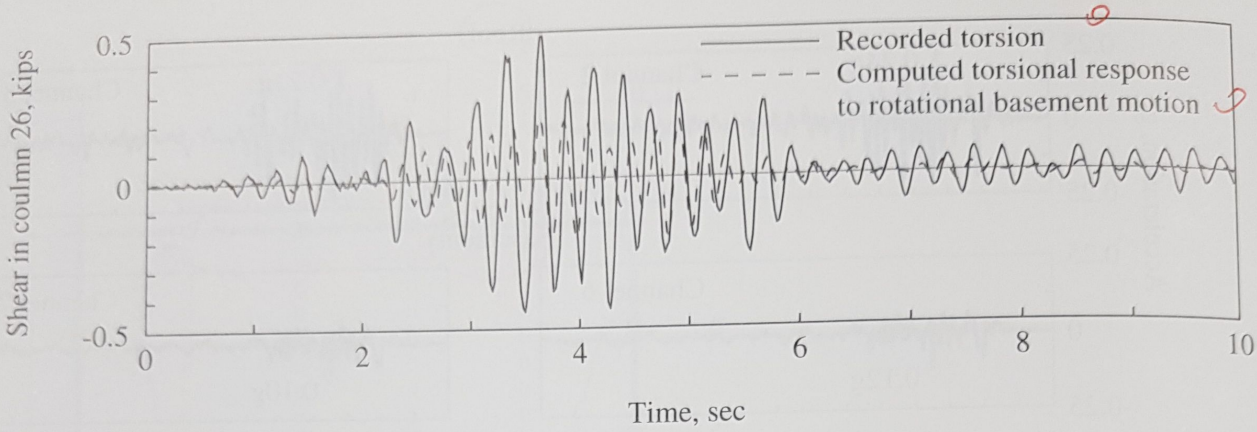

Figure 13.4.7 Comparison of shear force (x-component) in column 26 due to recorded torsion of the building and computed torsional response of the building to rotational basement motion. [From De la Llera and Chopra (1994).]

$\ddot{u}^t_{j\theta}$ is the torsional acceleration of the jth floor diaphragm. By using these inertia forces as equivalent static forces, we have included the damping forces and this is a source of approximation (see the last paragraph of Section 1.8.2). The results of these static analyses for the shear force in the same column are also presented in Fig. 13.4.7.

This figure show that the peak force due to rotational basement motion is about 45% of the peak force due to the actual torsional motion of the building. The remaining 55% of the force arises, in part, because this building is not *perfectly* symmetric due to several factors, the most obvious of them being the stairwell system shown in Fig. 13.4.2, and because the basement, which is under one-half of the floor plan, is not symmetrically located.

Torsional motion of buildings with nominally symmetric plan, such as the building of Fig. 13.4.1, is usually called *accidental torsion*. Such motion contributes a small fraction of the total earthquake forces in the structure. For the building and earthquake considered, accidental torsion contributed about 4% of the total force (results not presented here), but larger contributions have been identified in the earthquake response of other buildings. The structural response associated with accidental torsion is not amenable to calculation in structural design for two reasons: (1) the rotational base motion is not defined, and (2) it is not practical to identify and analyze the effect of each source of asymmetry in a building with nominally symmetric plan. Therefore, building codes include a simple design provision to account for accidental torsion in symmetric and unsymmetric buildings; in the latter case it is considered in addition to torsion arising from plan asymmetry (Section 13.3). Research has demonstrated deficiencies in this code provision.

13.5 RESPONSE ANALYSIS FOR MULTIPLE SUPPORT EXCITATION

In this section the modal analysis procedure of Section 13.1 is extended to MDF systems excited by prescribed motions $\ddot{u}_{gl}(t)$ at the various supports ($l = 1, 2, \ldots, N_g$) of the structure. In Section 9.7 the governing equations were shown to be the same as Eq. (13.1.1),

amplitudes of motion expected during the earthquake should be included in the structural idealization; and their stiffness properties should be determined using realistic assumptions. Similarly, as discussed in Chapter 11, selection of damping values for analysis of a structure should be based on available data from recorded earthquake responses of similar structures.

PART B: RESPONSE SPECTRUM ANALYSIS

13.7 PEAK RESPONSE FROM EARTHQUAKE RESPONSE SPECTRUM

The response history analysis (RHA) procedure presented in Part A provides structural response $r(t)$ as a function of time, but structural design is usually based on the peak values of forces and deformations over the duration of the earthquake-induced response. Can the peak response be determined directly from the response spectrum for the ground motion without carrying out a response history analysis? For SDF systems the answer to this question is yes (Chapter 6). However, for MDF systems the answer is a qualified yes. The peak response of MDF systems can be calculated from the response spectrum, but the result is not exact—in the sense that it is not identical to the RHA result; the estimate obtained is accurate enough for structural design applications, however. In Part B we present such response spectrum analysis (RSA) procedures for structures excited by a single component of ground motion; thus simultaneous action of the other two components is excluded and multiple support excitation is not considered. However, these more general cases have been solved by researchers and the interested reader should consult the published literature.

13.7.1 Peak Modal Responses

The peak value r_{no} of the nth-mode contribution $r_n(t)$ to response $r(t)$ can be obtained from the earthquake response spectrum or design spectrum. This becomes evident from Eq. (13.1.11) by recalling that the peak value of $A_n(t)$ is available from the pseudo-acceleration spectrum as its ordinate $A(T_n, \zeta_n)$, denoted as A_n, for brevity. Therefore,

$$r_{no} = r_n^{\text{st}} A_n \tag{13.7.1}$$

The algebraic sign of r_{no} is the same as that of r_n^{st} because A_n is positive by definition. Although it has an algebraic sign, r_{no}[†] will be referred to as the *peak modal response* because it corresponds to the peak value of $A_n(t)$. This algebraic sign must be retained because it can be important, as will be seen in Section 13.7.2. All response quantities $r_n(t)$ associated with a particular mode, say the nth mode, reach their peak values at the same

[†]This notation r_{no} should not be confused with the use of a subscript o in Chapter 6 to denote the maximum (over time) of the absolute value of the response quantity, which is positive by definition.

time instant as $A_n(t)$ reaches its peak (see Figs. 13.2.6 to 13.2.8, 13.2.10, 13.2.11, and E13.8a–d).

13.7.2 Modal Combination Rules

How do we combine the peak modal responses r_{no} $(n = 1, 2, \ldots, N)$ to determine the peak value $r_o \equiv \max_t |r(t)|$ of the total response? It will not be possible to determine the exact value of r_o from r_{no} because, in general, the modal responses $r_n(t)$ attain their peaks at different time instants and the combined response $r(t)$ attains its peak at yet a different instant. This phenomenon can be observed in Fig. 13.2.7b, where results for the shear in the top story of a five-story frame are presented. The individual modal responses $V_{sn}(t), n = 1, 2, \ldots, 5$, are shown together with the total response $V_s(t)$.

Approximations must be introduced in combining the peak modal responses r_{no} determined from the earthquake response spectrum because no information is available when these peak modal values occur. The assumption that all modal peaks occur at the same time and their algebraic sign is ignored provides an upper bound to the peak value of the total response:

$$r_o \le \sum_{n=1}^{N} |r_{no}| \qquad \text{(upper bound)} \tag{13.7.2}$$

This upper-bound value is usually too conservative, as we shall see in example computations to be presented later. Therefore, this *absolute sum* (ABSSUM) modal combination rule is not popular in structural design applications.

The *square-root-of-sum-of-squares* (SRSS) rule for modal combination, developed in E. Rosenblueth's Ph.D. thesis (1951), is

$$r_o \simeq \left(\sum_{n=1}^{N} r_{no}^2 \right)^{1/2} \tag{13.7.3}$$

The peak response in each mode is squared, the squared modal peaks are summed, and the square root of the sum provides an estimate of the peak total response. As will be seen later, this modal combination rule provides excellent response estimates for structures with well-separated natural frequencies. This limitation has not always been recognized in applying this rule to practical problems, and at times it has been misapplied to systems with closely spaced natural frequencies, such as piping systems in nuclear power plants and multistory buildings with unsymmetric plan.

The *complete quadratic combination* (CQC) rule for modal combination is applicable to a wider class of structures as it overcomes the limitations of the SRSS rule. According to the CQC rule,

$$r_o \simeq \left(\sum_{i=1}^{N} \sum_{n=1}^{N} \rho_{in} r_{io} r_{no} \right)^{1/2} \tag{13.7.4}$$

Each of the N^2 terms on the right side of this equation is the product of the peak responses in the ith and nth modes and the correlation coefficient ρ_{in} for these two modes; ρ_{in} varies

between 0 and 1 and $\rho_{in} = 1$ for $i = n$. Thus Eq. (13.7.4) can be rewritten as

$$r_o \simeq \left(\sum_{n=1}^{N} r_{no}^2 + \sum_{\substack{i=1 \\ i \neq n}}^{N} \sum_{n=1}^{N} \rho_{in} r_{io} r_{no} \right)^{1/2} \tag{13.7.5}$$

to show that the first summation on the right side is identical to the SRSS combination rule of Eq. (13.7.3); each term in this summation is obviously positive. The double summation includes all the cross ($i \neq n$) terms; each of these terms may be positive or negative. A cross term is negative when the modal static responses r_i^{st} and r_n^{st} assume opposite signs—for the algebraic sign of r_{no} is the same as that of r_n^{st} because A_n is positive by definition. Thus the estimate for r_o obtained by the CQC rule may be larger or smaller than the estimate provided by the SRSS rule. [It can be shown that the double summation inside the parentheses of Eq. (13.7.4) is always positive.]

Starting in the late 1960s and continuing through the 1970s and early 1980s, several formulations for the peak response to earthquake excitation were published. Some of these are identical or similar to Eq. (13.7.4) but differ in the mathematical expressions given for the correlation coefficient. Here we include two: one due to E. Rosenblueth and J. Elorduy for historical reasons because it was apparently the earliest (1969) result; and a second (1981) due to A. Der Kiureghian because it is now widely used.

The 1971 textbook *Fundamentals of Earthquake Engineering* by N. M. Newmark and E. Rosenblueth gives the Rosenblueth–Elorduy equations for the correlation coefficient:

$$\rho_{in} = \frac{1}{1 + \epsilon_{in}^2} \tag{13.7.6}$$

where

$$\epsilon_{in} = \frac{\omega_i \sqrt{1 - \zeta_i^2} - \omega_n \sqrt{1 - \zeta_n^2}}{\zeta_i' \omega_i + \zeta_n' \omega_n} \qquad \zeta_n' = \zeta_n + \frac{2}{\omega_n s} \tag{13.7.7}$$

and s is the duration of the strong phase of the earthquake excitation. Equations (13.7.6) and (13.7.7) show that $\rho_{in} = \rho_{ni}$; $0 \leq \rho_{in} \leq 1$; and $\rho_{in} = 1$ for $i = n$ or for two modes with equal frequencies and equal damping ratios. It is instructive to specialize Eq. (13.7.6) for systems with the same damping ratio in all modes subjected to earthquake excitation with duration s long enough to replace Eq. (13.7.7b) by $\zeta_n' = \zeta_n$. We substitute $\zeta_i = \zeta_n = \zeta$ in Eq. (13.7.7a), introduce $\beta_{in} = \omega_i / \omega_n$, and insert Eq. (13.7.7a) in Eq. (13.7.6) to obtain

$$\rho_{in} = \frac{\zeta^2 (1 + \beta_{in})^2}{(1 - \beta_{in})^2 + 4\zeta^2 \beta_{in}} \tag{13.7.8}$$

The equation for the correlation coefficient due to Der Kiureghian is

$$\rho_{in} = \frac{8\sqrt{\zeta_i \zeta_n}(\beta_{in}\zeta_i + \zeta_n)\beta_{in}^{3/2}}{(1 - \beta_{in}^2)^2 + 4\zeta_i \zeta_n \beta_{in}(1 + \beta_{in}^2) + 4(\zeta_i^2 + \zeta_n^2)\beta_{in}^2} \tag{13.7.9}$$

This equation also implies that $\rho_{in} = \rho_{ni}$, $\rho_{in} = 1$ for $i = n$ or for two modes with equal frequencies and equal damping ratios. For equal modal damping $\zeta_i = \zeta_n = \zeta$ this equation

simplifies to

$$\rho_{in} = \frac{8\zeta^2(1+\beta_{in})\beta_{in}^{3/2}}{(1-\beta_{in}^2)^2 + 4\zeta^2\beta_{in}(1+\beta_{in})^2} \tag{13.7.10}$$

Figure 13.7.1 shows Eqs. (13.7.8) and (13.7.10) for the correlation coefficient ρ_{in} plotted as a function of $\beta_{in} = \omega_i/\omega_n$ for four damping values: $\zeta = 0.02$, 0.05, 0.10, and 0.20. Observe that the two expressions give essentially identical values for ρ_{in}, especially in the neighborhood of $\beta_{in} = 1$, where ρ_{in} is the most significant.

This figure also provides an understanding of the correlation coefficient. Observe that this coefficient diminishes rapidly as the two natural frequencies ω_i and ω_n move farther apart. This is especially the case at small damping values that are typical of structures. In other words, it is only in a narrow range of β_{in} around $\beta_{in} = 1$ that ρ_{in} has significant values; and this range depends on damping. For example, $\rho_{in} > 0.1$ for systems with 5% damping over the frequency ratio range $1/1.35 \leq \beta_{in} \leq 1.35$. If the damping is 2%, this range is reduced to $1/1.18 \leq \beta_{in} \leq 1.18$. For structures with well-separated natural frequencies the coefficients ρ_{in} vanish; as a result all cross ($i \neq n$) terms in the CQC rule, Eq. (13.7.5), can be neglected and it reduces to the SRSS rule, Eq. (13.7.3). It is now clear

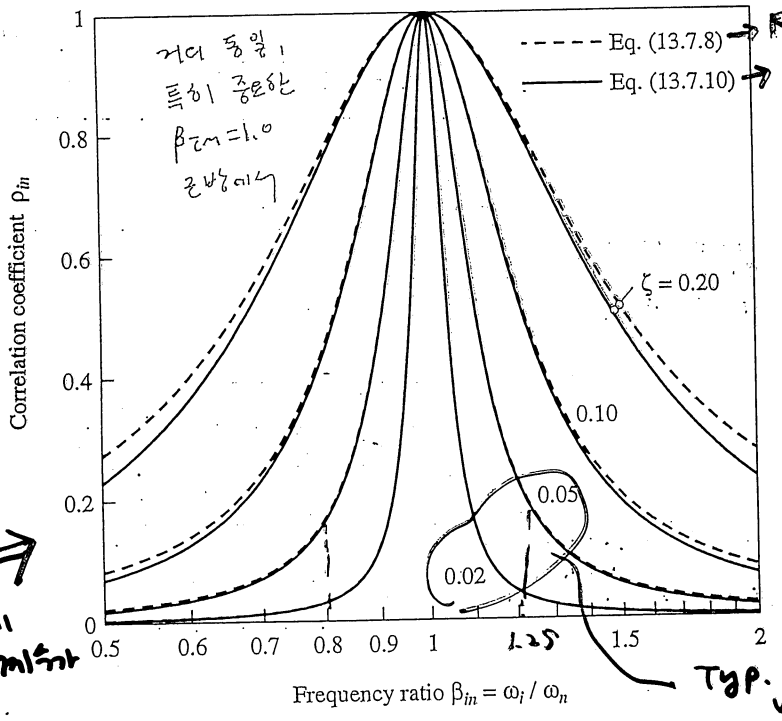

Figure 13.7.1 Variation of correlation coefficient ρ_{in} with modal frequency ratio, $\beta_{in} = \omega_i/\omega_n$, as given by two different equations for four damping values; abcissa scale is logarithmic.

that the SRSS rule applies to structures with well-separated natural frequencies of those modes that contribute significantly to the response.

The SRSS and CQC rules for combination of peak modal responses have been presented without the underlying derivations based on random vibration theory, a subject beyond the scope of this book. It is important, however, to recognize the implications of the assumptions behind the derivations. These assumptions indicate that the modal combination rules would be most accurate for earthquake excitations that contain a wide band of frequencies with long phases of strong shaking, which are several times longer than the fundamental periods of the structures, which are not too lightly damped ($\zeta_n > 0.005$). In particular, these modal combination rules will become less accurate for short-duration impulsive ground motions and are not recommended for ground motions that contain many cycles of essentially harmonic excitation.

Considering that the SRSS and CQC modal combination rules are based on random vibration theory, r_{no} should be interpreted as the mean of the peak values of response to an ensemble of earthquake excitations. Thus the modal combination rules are intended for use when the excitation is characterized by a smooth response (or design) spectrum, based on the response spectra for many earthquake excitations. The smooth spectrum may be the mean or median of the individual response spectra or it may be a more conservative spectrum, such as the mean-plus-one-standard-deviation spectrum (Section 6.9). The CQC or SRSS modal combination rule (as appropriate depending on the closeness of natural frequencies) when used in conjunction with, say, the mean spectrum provides an estimate of the peak response that is reasonably close to the mean of the peak values of response to individual excitations. The error in the estimate of the peak may be on either side, conservative or unconservative, and is usually no more than several percent for typical structures and earthquakes; see examples later.

It has been found that Eq. (13.7.3) or (13.7.4) also approximates the peak response to a single ground motion characterized by a jagged response spectrum. The errors are larger, however, in this case: perhaps in the range of 10 to 30%, depending on the fundamental period of the structure; see examples later.

13.7.3 Interpretation of Response Spectrum Analysis

The response spectrum analysis (RSA) described in the preceding section is a procedure for dynamic analysis of a structure subjected to earthquake excitation, but it reduces to a series of static analyses. For each mode considered, static analysis of the structure subjected to forces $\mathbf{s}_n$ provides the modal static response r_n^{st}, which is multiplied by the spectral ordinate A_n to obtain the peak modal response r_{no} [Eq. (13.7.1)]. Thus the RSA procedure avoids the dynamic analysis of SDF systems necessary for response history analysis (Fig. 13.1.1). However, the RSA is still a dynamic analysis procedure because it uses the vibration properties—natural frequencies, natural modes, and modal damping ratios—of the structure and the dynamic characteristics of the ground motion through its response (or design) spectrum. It is just that the user does not have to carry out any response history calculations; somebody has already done these in developing the earthquake response spectrum or the earthquake excitation has been characterized by a smooth design spectrum.

13.8 MULTISTORY BUILDINGS WITH SYMMETRIC PLAN

13.8.1 Response Spectrum Analysis Procedure

In this section the response spectrum analysis procedure of Section 13.7 is specialized for multistory buildings with their plans having two axes of symmetry subjected to horizontal ground motion along one of these axes. The peak value† of the nth-mode contribution $r_n(t)$ to a response quantity is given by Eq. (13.7.1). The modal static response r_n^{st} is calculated by static analysis of the building subjected to lateral forces $\mathbf{s}_n$ of Eq. (13.2.4). Equations for r_n^{st} for several response quantities are available in Table 13.2.1. Substituting these formulas for floor displacement u_j, story drift Δ_j, base shear V_b, and base overturning moment M_b in Eq. (13.7.1) gives

$$u_{jn} = \Gamma_n \phi_{jn} D_n \qquad \Delta_{jn} = \Gamma_n (\phi_{jn} - \phi_{j-1,n}) D_n \tag{13.8.1a}$$

$$V_{bn} = M_n^* A_n \qquad M_{bn} = h_n^* M_n^* A_n \tag{13.8.1b}$$

where $D_n \equiv D(T_n, \zeta_n)$, the deformation spectrum ordinate corresponding to natural period T_n and damping ratio ζ_n; $D_n = A_n/\omega_n^2$.

Equations (13.8.1) for the peak modal responses are equivalent to static analysis of the building subjected to the equivalent static forces associated with the nth-mode peak response:

$$\mathbf{f}_n \equiv \mathbf{s}_n A_n \qquad f_{jn} = \Gamma_n m_j \phi_{jn} A_n \tag{13.8.2}$$

where $\mathbf{f}_n$ is the vector of forces f_{jn} at the various floor levels, $j = 1, 2, \ldots, N$ (Fig. 13.8.1); $\mathbf{s}_n$ is defined by Eq. (13.2.4). The force vector $\mathbf{f}_n$ is the peak value of $\mathbf{f}_n(t)$, obtained by

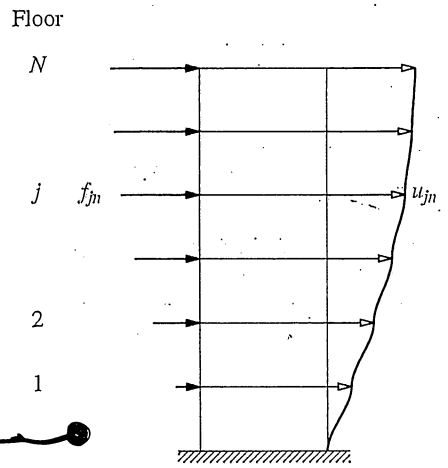

Figure 13.8.1 Peak values of lateral displacements and equivalent static lateral forces associated with the nth mode.

†From now on, the subscript o is dropped from r_o for brevity [i.e., $\bar{r}$ will denote the peak value of $r(t)$].

replacing $A_n(t)$ in Eq. (13.2.7) by the spectral ordinate A_n. Because only one static analysis is required for each mode, it is more direct to do so for the forces $\mathbf{f}_n$ instead of $\mathbf{s}_n$ and then multiplying the latter results by A_n. In contrast, the use of the modal static response r_n^{st} was emphasized in response history analysis because it highlighted the fact that the static analysis for forces $\mathbf{s}_n$ was needed only once even though the response was computed at many time instants.

Thus the peak value r_n of the nth-mode contribution to a response quantity r is determined by static analysis of the building due to lateral forces $\mathbf{f}_n$; the direction of forces f_{jn} is controlled by the algebraic sign of ϕ_{jn}. Hence these forces for the fundamental mode will act in the same direction (Fig. 13.8.1), but for the second and higher modes they will change direction as one moves up the building. Observe that this static analysis is not necessary to determine floor displacements or story drifts; Eq. (13.8.1a) provides the more convenient alternative. The peak value of the total response is estimated using the modal combination rules of Eq. (13.7.3) or (13.7.4), as appropriate, including all modes that contribute significantly to the response.

Summary. The procedure to compute the peak response of an N-story building with plan symmetric about two orthogonal axes to earthquake ground motion along an axis of symmetry, characterized by a response spectrum or design spectrum, is summarized in step-by-step form:

1. Define the structural properties.
   - **a.** Determine the mass matrix $\mathbf{m}$ and lateral stiffness matrix $\mathbf{k}$ (Section 9.4).
   - **b.** Estimate the modal damping ratios ζ_n (Chapter 11).
2. Determine the natural frequencies ω_n (natural periods $T_n = 2\pi/\omega_n$) and natural modes ϕ_n of vibration (Chapter 10).
3. Compute the peak response in the nth mode by the following steps to be repeated for all modes, $n = 1, 2, \ldots, N$:
   - **a.** Corresponding to natural period T_n and damping ratio ζ_n, read D_n and A_n, the deformation and pseudo-acceleration, from the earthquake response spectrum or the design spectrum.
   - **b.** Compute the floor displacements and story drifts from Eq. (13.8.1a).
   - **c.** Compute the equivalent static lateral forces $\mathbf{f}_n$ from Eq. (13.8.2).
   - **d.** Compute the story forces—shear and overturning moment—and element forces—bending moments and shears—by static analysis of the structure subjected to lateral forces $\mathbf{f}_n$.
4. Determine an estimate for the peak value r of any response quantity by combining the peak modal values r_n according to the SRSS rule, Eq. (13.7.3), if the natural frequencies are well separated. The CQC rule, Eq. (13.7.4), should be used if the natural frequencies are closely spaced.

Usually, only the lower modes contribute significantly to the response. Therefore, steps 2 and 3 need to be implemented for only these modes and the modal combinations of Eqs. (13.7.3) and (13.7.4) truncated accordingly.

How many modes to combine?

: 통상 90% Effective modal mass rule

$M_n^* = \Gamma_n L_n$

(See Table 13.2.1, P. 518
Figure 13.2.5, P. 527)

Example 13.11

The peak response of the two-story frame of Example 13.4, shown in Fig. E13.11a, to ground motion characterized by the design spectrum of Fig. 6.9.5 scaled to 0.5g peak ground acceleration is to be determined. This reinforced-concrete frame has the following properties: $E = 3 \times 10^3$ ksi, $I = 1000$ in^4, $h = 10$ ft, $L = 20$ ft. Determine the lateral displacements of the frame and bending moments at both ends of each beam and column.

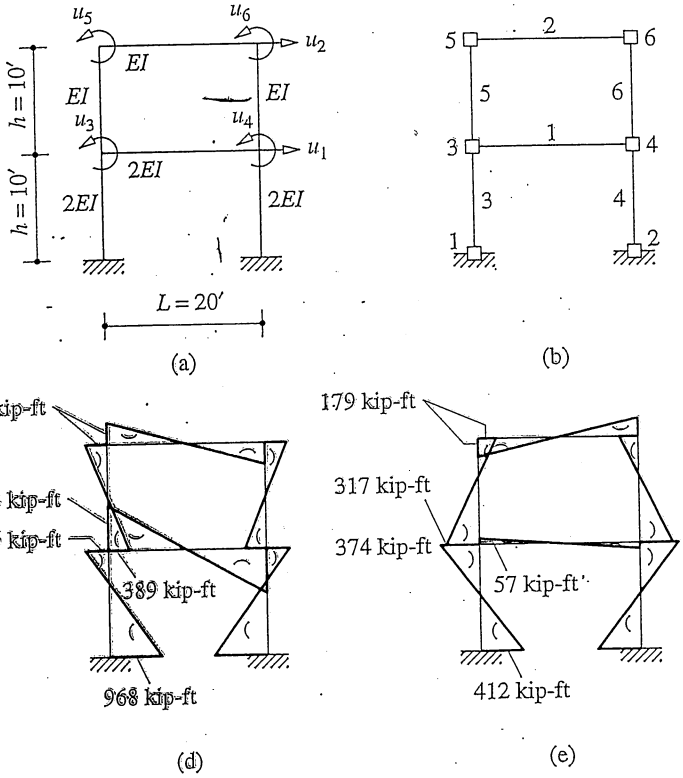

Figure E13.11

Solution Steps 1 and 2 of the summary have already been implemented and the results are available in Examples 10.5 and 13.4. Substituting for E, I, and h in Eq. (b) of Example 13.4 gives ω_n and $T_n = 2\pi/\omega_n$:

$$\omega_1 = 4.023 \qquad \omega_2 = 10.71 \text{ rad/sec}$$

$$T_1 = 1.562 \qquad T_2 = 0.5868 \text{ sec}$$

Step 3a: Corresponding to these periods, the spectral ordinates are $D_1 = 13.72$ in. and $D_2 = 4.578$ in.

1. *Determine the floor displacements.*

Step 3b: Using Eq. (13.8.1a) with numerical values for Γ_n and ϕ_{jn} from Example 13.4 and D_n from step 3(a) gives the peak displacements $\mathbf{u}_n$ due to the two modes:

$$\mathbf{u}_1 = \begin{Bmatrix} u_1 \\ u_2 \end{Bmatrix}_1 = 1.365 \begin{Bmatrix} 0.3871 \\ 1 \end{Bmatrix} 13.72 = \begin{Bmatrix} 7.252 \\ 18.73 \end{Bmatrix} \text{in.}$$

$$\mathbf{u}_2 = \begin{Bmatrix} u_1 \\ u_2 \end{Bmatrix}_2 = -0.365 \begin{Bmatrix} -1.292 \\ 1 \end{Bmatrix} 4.578 = \begin{Bmatrix} 2.159 \\ -1.672 \end{Bmatrix} \text{in.}$$

Step 4: Using the SRSS rule for modal combination, estimates for the peak values of the floor displacements are

$$u_1 \simeq \sqrt{(7.252)^2 + (2.159)^2} = 7.566 \text{ in.}$$

$$u_2 \simeq \sqrt{(18.73)^2 + (-1.672)^2} = 18.81 \text{ in.}$$

2. *Determine the element forces.* Instead of implementing steps 3c and 3d as described in the summary, here we illustrate the computation of element forces from the floor displacements and joint rotations. The elements and nodes are numbered as shown in Fig. E13.11b.

First mode. Joint rotations are obtained from Eq. (d) of Example 9.9 with $\mathbf{u}_t$ replaced by $\mathbf{u}_1$:

$$\mathbf{u}_{01} = \begin{Bmatrix} u_3 \\ u_4 \\ u_5 \\ u_6 \end{Bmatrix}_1 = \frac{1}{120} \begin{bmatrix} -0.4426 & -0.2459 \\ -0.4426 & -0.2459 \\ 0.9836 & -0.7869 \\ 0.9836 & -0.7869 \end{bmatrix} \begin{bmatrix} 7.252 \\ 18.73 \end{bmatrix} = \begin{bmatrix} -6.514 \\ -6.514 \\ -6.340 \\ -6.340 \end{bmatrix} \times 10^{-2}$$

From $\mathbf{u}_1$ and $\mathbf{u}_{01}$ all element forces can be calculated. For example, the bending moment at the left end of the first floor beam (Fig. E13.11c) is

$$M_a = \frac{4EI}{L}\theta_a + \frac{2EI}{L}\theta_b + \frac{6EI}{L^2}u_a - \frac{6EI}{L^2}u_b$$

Substituting $E = 3 \times 10^3$ ksi, $I = 2000$ in^4, $L = 240$ in., $\theta_a = u_3$, $\theta_b = u_4$, $u_a = u_b = 0$ gives $M_a = -9770$ kip-in. $= -814$ kip-ft. Bending moments in all elements can be calculated similarly. The results are summarized in Table E13.11 and in Fig. E13.11d.

TABLE E13.11 PEAK BENDING MOMENTS (KIP-FT)

Element	Node	Mode 1	Mode 2	SRSS
Beam 1	3	−814	−57	816
	4	−814	−57	816
Beam 2	5	−396	179	435
	6	−396	179	435
Column 3	3	425	374	566
	1	968	412	1052
Column 5	5	396	−179	435
	3	389	−317	502

Second mode. Joint rotations $\mathbf{u}_{02}$ are obtained from Eq. (d) of Example 9.9 with $\mathbf{u}_1$ replaced by $\mathbf{u}_2$. Computations for the element forces parallel those shown for the first mode, but using $\mathbf{u}_2$ and $\mathbf{u}_{02}$, leading to the results in Table E13.11 and in Fig. E13.11e.

Step 4: The peak value of each element force is estimated by combining its peak modal values by the SRSS rule. The results are shown in Table E13.11. Note that the algebraic signs of the bending moments are lost in the total values; therefore, it is not meaningful to draw the bending moment diagram and the total moments do not satisfy equilibrium at joints.

13.8.2 Example: Five-Story Shear Frame

In this section the RSA procedure is implemented for the five-story shear frame of Fig. 12.8.1. The complete history of this structure's response to the El Centro ground motion was determined in Section 13.2.6. We now estimate its peak response directly from the response spectrum for this excitation (i.e., without computing its response history).

Presented in Sections 12.8 and 13.2.6 were the mass and stiffness matrices and the natural vibration periods and modes of this structure. From these data, the modal properties M_n and L_n^h were computed (Table 13.2.2). The damping ratios are estimated as $\zeta_n = 5\%$.

Response spectrum ordinates. The response spectrum for the El Centro ground motion for 5% damping gives the values of D_n and A_n noted in Fig. 13.8.2 corresponding to the natural periods T_n. These are the precise values for the spectral ordinates, the peak values of $D_n(t)$ and $A_n(t)$ in Fig. 13.2.6, thus eliminating any errors in reading spectral ordinates. Such errors are inherent in practical implementation of the RSA procedure with a jagged response spectrum, but are eliminated if a smooth design spectrum, such as Fig. 6.9.5, is used.

Peak modal responses. The floor displacements are determined from Eq. (13.8.1a) using known values of ϕ_{jn} (Section 12.8), of L_n^h (Table 13.2.2) and $\Gamma_n = L_n^h$ (because $M_n = 1$), and of D_n (Fig. 13.8.2). For example, the floor displacements due to the first mode are computed as follows:

$$\mathbf{u}_1 = \Gamma_1 \phi_1 D_1 = 1.067 \begin{Bmatrix} 0.334 \\ 0.641 \\ 0.895 \\ 1.078 \\ 1.173 \end{Bmatrix} 5.378 = \begin{Bmatrix} 1.916 \\ 3.677 \\ 5.139 \\ 6.188 \\ 6.731 \end{Bmatrix} \text{in.}$$

These displacements are shown in Fig. 13.8.3a. The equivalent static forces for the nth mode are computed from Eq. (13.8.2) using known values of Γ_n, ϕ_{jn}, $m_j = m = 100$ kips/g, and A_n (Fig. 13.8.2). For example, the forces associated with the first mode are computed as follows:

$$\mathbf{f}_1 = \Gamma_1 \begin{Bmatrix} m_1\phi_{11} \\ m_2\phi_{21} \\ m_3\phi_{31} \\ m_4\phi_{41} \\ m_5\phi_{51} \end{Bmatrix} A_1 = 1.067 \frac{100}{g} \begin{Bmatrix} 0.334 \\ 0.641 \\ 0.895 \\ 1.078 \\ 1.173 \end{Bmatrix} 0.1375g = \begin{Bmatrix} 4.899 \\ 9.401 \\ 13.141 \\ 15.817 \\ 17.211 \end{Bmatrix} \text{kips}$$

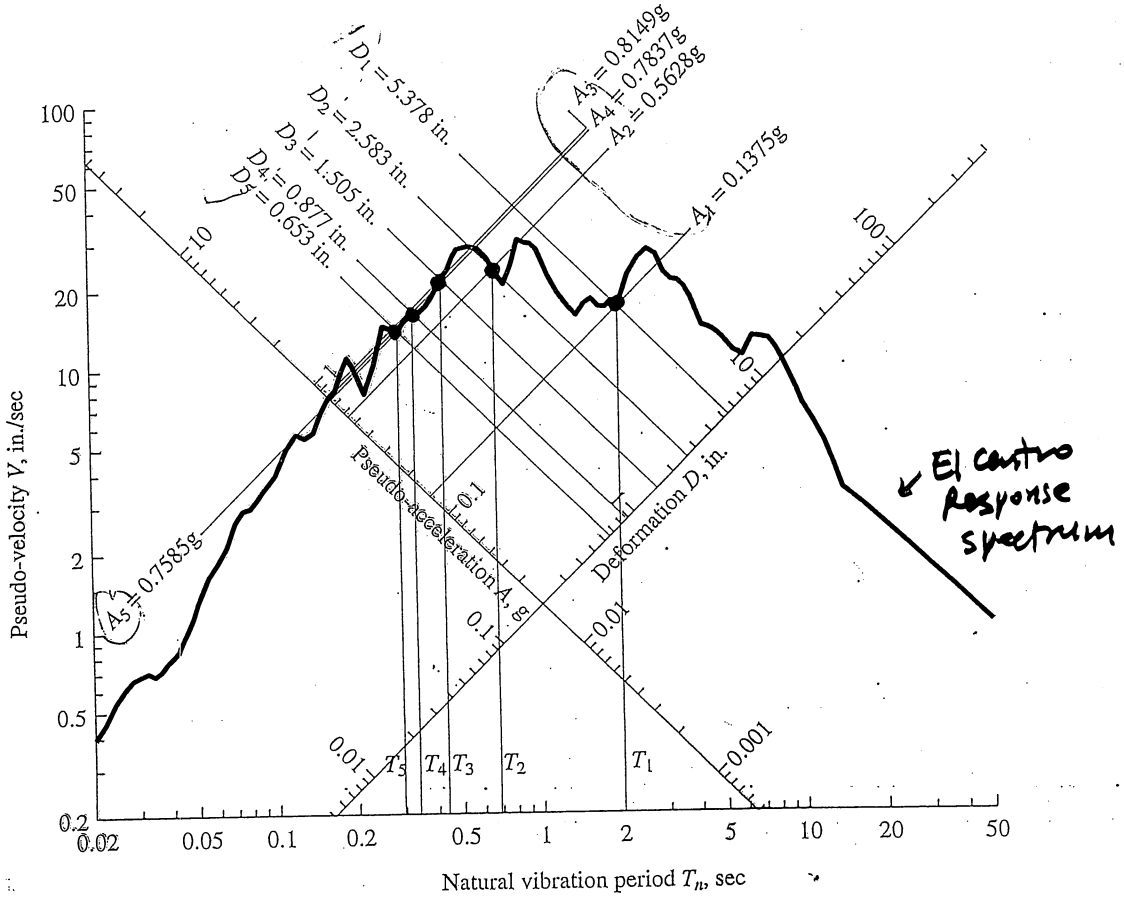

Figure 13.8.2 Earthquake response spectrum with natural vibration periods T_n of example structure shown together with spectral values D_n and A_n.

These forces are also shown in Fig. 13.8.3a. Alternatively, $\mathbf{f}_n$ can be computed by multiplying known values of $\mathbf{s}_n$ (Fig. 13.2.4) by A_n (Fig. 13.8.2). Repeating these computations for modes $n = 2$, 3, 4, and 5 leads to the remaining results of Fig. 13.8.3. Observe that the equivalent static forces for the first mode all act in the same direction, but for the second and higher modes they change direction as one moves up the building; the direction of forces is controlled by the algebraic sign of ϕ_{jn} (Fig. 12.8.2).

For each mode the peak value of any story force or element force is computed by static analysis of the structure subjected to the equivalent static lateral forces $\mathbf{f}_n$. Table 13.8.1 summarizes these peak values for the base shear V_b, top-story shear V_5, and base overturning moment M_b. The earlier data for roof displacement u_5 are also included. These peak modal values are exact because the errors in reading spectral ordinates had been eliminated in this example. This is apparent by comparing the data in Table 13.8.1

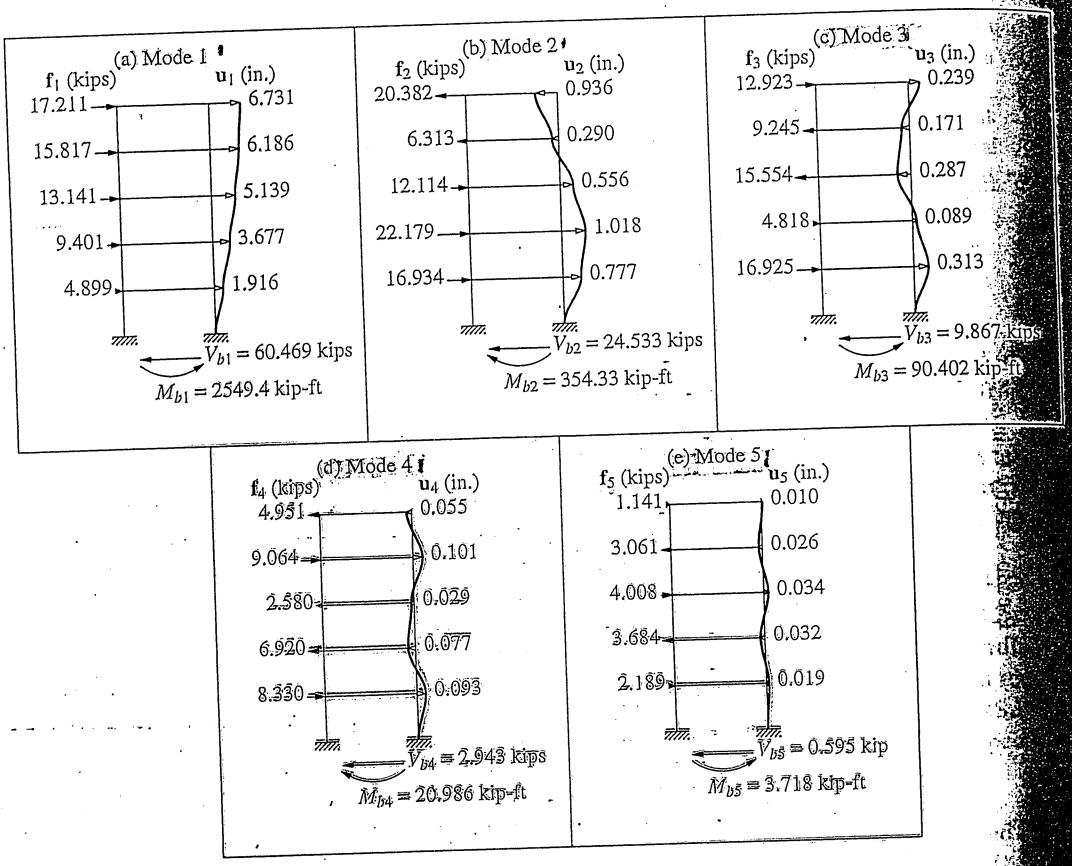

Figure 13.8.3 Peak values of displacements and equivalent static lateral forces due to the five natural vibration modes.

and the peak modal values from response history analysis in Figs. 13.2.7 and 13.2.8. The two sets of data agree except possibly for their algebraic signs because the peak values D_n and A_n are positive by definition.

Alternatively, Eq. (13.7.1) could have been used for computing the peak modal response. For example, the modal static responses V_{bn}^{st} and M_{bn}^{st} are available from

TABLE 13.8.1 PEAK MODAL RESPONSES

Mode	V_b (kips)	V_5 (kips)	M_b (kip-ft)	u_5 (in.)
1	60.469	17.211	2549.4	6.731
2	24.533	−20.382	−354.33	−0.936
3	9.867	12.923	90.402	0.239
4	2.943	−4.951	−20.986	−0.055
5	0.595	1.141	3.718	0.010

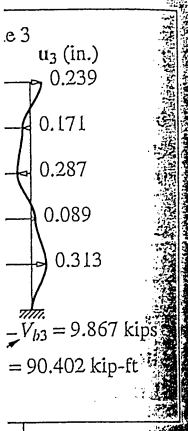

the five natural

and 13.2.8. The
peak values D_n

the peak modal
available from

Table 13.2.3 and A_n from Fig. 13.8.2. For example, the first-mode calculations are

$$V_{b1} = V_{b1}^{st} A_1 = [4.398(100/g)]0.1375g = 60.469 \text{ kips}$$

$$M_{b1} = M_{b1}^{st} A_1 = [(15.45)(100/g)12]0.1375g = 2549.4 \text{ kip-ft}$$

As expected, these are the same as the data in Table 13.8.1.

Modal combination. The peak value r of the total response $r(t)$ is estimated by combining the peak modal responses according to the ABSSUM, SRSS, and CQC rules of Eqs. (13.7.2) to (13.7.4). Their use is illustrated for one response quantity, the base shear.

The ABSSUM rule of Eq. (13.7.2) is specialized for the base shear:

$$V_b \le \sum_{n=1}^{5} |V_{bn}| \tag{13.8.3}$$

Substituting for the known values of V_{bn} from Table 13.8.1 gives

too conservative

$$V_b \le 60.469 + 24.533 + 9.867 + 2.943 + 0.595 \quad \text{or} \quad V_b \le 98.407 \text{ kips}$$

As expected, the ABSSUM estimate of 98.407 kips is much larger than the exact value of 73.278 kips (Fig. 13.2.7).

The SRSS rule of Eq. (13.7.3) is specialized for the base shear:

$$V_b \simeq \left(\sum_{n=1}^{5} V_{bn}^2 \right)^{1/2} \tag{13.8.4}$$

Substituting for the known values of V_{bn} from Table 13.8.1 gives

$$V_b \simeq \sqrt{(60.469)^2 + (24.533)^2 + (9.867)^2 + (2.943)^2 + (0.595)^2} = 66.066 \text{ kips} \simeq V_{b1}$$

Observe that the contributions of modes higher than the second are small.

The CQC rule of Eq. (13.7.4) is specialized for the base shear:

$$V_b \simeq \left(\sum_{i=1}^{5} \sum_{n=1}^{5} \rho_{in} V_{bi} V_{bn} \right)^{1/2} \tag{13.8.5}$$

Needed in this equation are the correlation coefficients ρ_{in}, which depend on the frequency ratios $\beta_{in} = \omega_i/\omega_n$, computed from the known natural frequencies (Section 13.2.6) and repeated in Table 13.8.2 for convenience.

$\beta_{in} = \dfrac{\omega_n}{\omega_i}$

TABLE 13.8.2 NATURAL FREQUENCY RATIOS β_{in}

Mode, i	$n=1$	$n=2$	$n=3$	$n=4$	$n=5$	ω_i (rad/sec)
1	1.000	0.343	0.217	0.169	0.148	3.1416
2	2.919	1.000	0.634	0.494	0.433	9.1703
3	4.602	1.576	1.000	0.778	0.683	14.4561
4	5.911	2.025	1.285	1.000	0.877	18.5708
5	6.742	2.310	1.465	1.141	1.000	21.1810

well-separated
(각각 분리됨)

TABLE 13.8.3 CORRELATION COEFFICIENTS ρ_{in}

Mode, i	$n=1$	$n=2$	$n=3$	$n=4$	$n=5$
1	1.000	0.007	0.003	0.002	0.001
2	0.007	1.000	0.044	0.018	0.012
3	0.003	0.044	1.000	0.136	0.062
4	0.002	0.018	0.136	1.000	0.365
5	0.001	0.012	0.062	0.365	1.000

TABLE 13.8.4 INDIVIDUAL TERMS IN CQC RULE: BASE SHEAR V_b

Mode, i	$n=1$	$n=2$	$n=3$	$n=4$	$n=5$
1	3656.476	10.172	1.615	0.306	0.049
2	10.172	601.844	10.687	1.284	0.178
3	1.615	10.687	97.354	3.943	0.365
4	0.306	1.284	3.943	8.658	0.639
5	0.049	0.178	0.365	0.639	0.354

For each β_{in} value in Table 13.8.2, ρ_{in} is determined from Eq. (13.7.10) for $\zeta = 0.05$ and presented in Table 13.8.3. Observe that the cross-correlation coefficients ρ_{in} $(i \neq n)$ are small because the natural frequencies of the five-story shear frame are well separated.

The 25 terms in the double summation of Eq. (13.8.5), computed using the known values of ρ_{in} (Table 13.8.3) and V_{bn} (Table 13.8.1), are given in Table 13.8.4. Adding these 25 terms and taking the square root gives $V_b \simeq 66.507$ kips. It is clear that only the $i = n$ terms are significant and the cross-terms $(i \neq n)$ are small because the cross-correlation coefficients are small. Note that the contributions of modes higher than the second mode could be neglected, thus reducing the computational effort.

Comparison of RSA and RHA results. The RSA estimates of peak response obtained from the ABSSUM, SRSS, and CQC rules are summarized in Table 13.8.5 together with the RHA results from Figs. 13.2.7 to 13.2.8. In the preceding section, computational details for estimating the peak base shear by RSA were presented; similarly, results for V_5, M_b, and u_5 were obtained. These data permit several observations. First, the ABSSUM rule can be excessively conservative and should therefore not be used. Second, the SRSS and CQC rules give essentially the same estimates of peak response because the cross-correlation coefficients are small for this structure with well-separated natural frequencies. Third, the peak responses estimated by SRSS or CQC rules are smaller than the RHA values; this is not a general trend, however, and larger values can also be estimated when using a jagged response spectrum for a single excitation. Fourth, the error in SRSS (or CQC) estimates of peak response, expressed as a percentage of the RHA value, vary with the response quantity. It is about 15% for the top-story shear V_5, 10% for the base shear V_b, and less than 1% for the base overturning moment M_b and top-floor displacement

TABLE 13.8.5 RSA AND RHA VALUES OF PEAK RESPONSE

	V_b (kips)	V_5 (kips)	M_b (kip-ft)	u_5 (in.)
ABSSUM	98.407	56.608	3018.8	7.971
SRSS	66.066	30.074	2575.6	6.800
CQC	66.507	29.338	2572.7	6.793
RHA	73.278	35.217	2593.2	6.847

u_5. The error is largest for V_5 because the responses due to the higher modes are most significant (compared to other response quantities considered) relative to the first mode (Table 13.8.1). Similarly, the error is smallest for M_b because the higher-mode responses are a very small fraction of the first-mode response (Table 13.8.1).

Now consider a typical application of the RSA procedure in which the peak response is estimated for excitations characterized by a smooth design spectrum, say the mean or median spectrum derived from individual spectra for many ground motions (Section 6.9). The error in this RSA estimate relative to the mean of the exact peak values (from response history analyses of the structure) for individual excitations will be generally much smaller than the errors noted above for a single excitation—perhaps no more than several percent.

Avoid a pitfall. Observe that the peak value r of each response quantity was determined by combining the peak values r_n of the modal contributions to the same response quantity. This is the correct way of estimating the peak value of a response quantity.

On the other hand, it is wrong to compute the combined peak value of one response quantity from the combined peak values of other response quantities. For example, it is desired to determine Δ_5, the drift in the fifth story of the building just analyzed. It is incorrect to determine its peak value from $\Delta_5 = u_5 - u_4$, where u_5 and u_4 have been determined by combining their modal peaks u_{5n} and u_{4n}, respectively. The correct procedure to determine Δ_5 is by combining the peak modal values, $\Delta_{5n} = u_{5n} - u_{4n}$.

Similarly, it is erroneous to compute the combined peak value of an internal force from the combined peak values of other forces. In particular, it is incorrect to determine the story shears or story overturning moments from the combined peak values of the equivalent static forces. The SRSS combination of the peak values of the equivalent static forces f_{jn} for each mode of the five-story shear building (Fig. 13.8.3) is shown in Fig. 13.8.4. Static

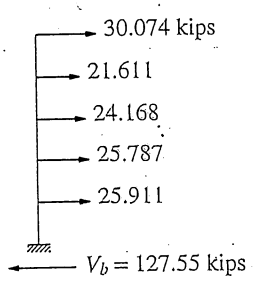

Figure 13.8.4 Wrong procedure for computing internal forces.

analysis of the structure with these external forces gives the base shear $V_b = 127.55$ kips, which is almost twice the correct SRSS value presented in Table 13.8.5. This erroneous value is much larger because the algebraic signs of f_{jn} (Fig. 13.8.3) are lost in the SRSS combination and the forces shown in Fig. 13.8.4 are all in the same direction.

13.8.3 Example: Four-Story Frame with an Appendage

This section is concerned with the four-story frame with a light appendage of Section 13.2.7, where its response history due to El Centro ground motion was presented. In this section the peak responses of the same structure are estimated by the RSA procedure directly from the response spectrum for the ground motion. The analysis procedure and the details of its implementation are identical to those described in Section 13.8.2. Therefore, only a summary of the results is presented.

Table 13.8.6 shows the natural periods T_n and the associated spectral ordinates for 5% damping together with the peak modal responses for two response quantities: base

TABLE 13.8.6 SPECTRAL VALUES AND PEAK MODAL RESPONSES

Mode	T_n (sec)	D_n (in.)	A_n/g	V_b (kips)	V_5 (kips)
1	2.000	5.378	0.1375	26.805	1.367
2	1.873	5.335	0.1556	25.429	−1.397
3	0.672	2.631	0.5950	19.816	0.027
4	0.439	1.545	0.8176	6.414	−0.005
5	0.358	0.928	0.7407	1.090	0.001

shear V_b and appendage shear V_5. The ratios β_{in} of natural frequencies are given in Table 13.8.7. The correlation coefficients computed by Eq. (13.7.10) for each β_{in} value are listed in Table 13.8.8.

TABLE 13.8.7 NATURAL FREQUENCY RATIOS β_{in}

Mode, i	$n=1$	$n=2$	$n=3$	$n=4$	$n=5$	ω_i (rad/sec)
1	1.000	0.936	0.336	0.219	0.179	3.142
2	1.068	1.000	0.359	0.234	0.191	3.355
3	2.974	2.785	1.000	0.653	0.532	9.344
4	4.556	4.266	1.532	1.000	0.815	14.314
5	5.589	5.233	1.879	1.227	1.000	17.558

★ How about inelastic dynamic analysis?

"elasto-plastic member properties" 이용하면 됨!

ex)

중요 lumped (concentrated) plastic hinge 부재끝 점